Remote Bathymetry of the Littoral Zone From AVIRIS, LASH, and QuickBird Imagery

Steven M. Adler-Golden, Prabhat K. Acharya, Alexander Berk, Michael W. Matthew, and David Gorodetzky

Abstract—**An efficient, physics-based remote bathymetry method for the littoral zone is described and illustrated with applications to QuickBird, Littoral Airborne Sensor: Hyperspectral (LASH), and Airborne Visible/Infrared Spectrometer (AVIRIS) spectral imagery. The method combines atmospheric correction, water reflectance spectral simulations, and a linear unmixing bathymetry algorithm that accounts for water surface reflections, thin clouds, and variable bottom brightness, and can incorporate blends of bottom materials. Results include depth maps, bottom color visualizations, and in favorable cases, approximate descriptions of the water composition. In addition, atmospheric correction was advanced through new capabilities added to the Fast Line-of-sight Atmospheric Analysis of Spectral Hypercubes (FLAASH) and Moderate Resolution Transmittance (MODTRAN) codes, including characterization of the aerosol wavelength dependence and a discrete-ordinate-method radiative transfer scaling technique for rapid calculation of multiply scattered radiance.**

Index Terms—**Algorithms, compensation, hydrology, hypercubes, optical image processing, remote sensing, satellite applications, sea coast, spectral analysis, underwater object detection.**

I. Introduction

REMOTE spectral imaging of the littoral zone (LZ) can provide valuable information for characterizing coastal waters. The use of multispectral imagery (MSI) from satellite sensors such as Landsat, the Sea-viewing Wide Field-of-view Sensor (SeaWIFS), the Moderate Resolution Imaging Spectroradiometer (MODIS), the Multi-angle Imaging SpectroRadiometer (MISR), and others has been established for many applications, including retrieving water chlorophyll and approximate water depth. With the advent of hyperspectral imaging (HSI) sensors such as the Airborne Visible/Infrared Spectrometer (AVIRIS), Hyperion, the Hyperspectral Mapper (HyMap), the Hyperspectral Digital Imagery Collection Experiment (HYDICE), and others, which typically cover the solar wavelength region ($\sim$0.4–2.5 μm) in $\sim 10^2$ or more spectral channels, there is the potential to retrieve much more information; applications include identifying and characterizing underwater objects and materials and mapping water depth to within a meter or better. However, achieving these goals requires overcoming a number of challenges. Water-leaving radiance is difficult to determine accurately, as it is often small compared to reflected radiance from sources such as atmospheric and water surface scattering, and it is subject to uncertainties in the sensor's radiometric calibration. Unknown bottom materials and water composition can reduce the bathymetry accuracy. In addition, limited "ground truth" bottom spectra and depths restrict the ability to evaluate performance of the retrieval algorithms.

This paper describes an efficient, physics-based remote bathymetry method for the LZ that uses minimal ground truth input, and presents results for three different hyperspectral and multispectral sensors at two locations. The data consist of QuickBird satellite and Littoral Airborne Sensor: Hyperspectral (LASH) aircraft-based imagery of Kaneohe Bay, HI, where recent, high spatial resolution ground-truth bathymetry data from the Scanning Hydrographic Operational Airborne Lidar Survey (SHOALS) lidar system are available, and a 20-km-altitude AVIRIS image of Tampa Bay, FL, where there are older bathymetry data from the National Ocean Service (NOS). Our method uses a first-principles atmospheric correction algorithm, described in Section II, and simulations of water reflectance spectra, described in Section III, together with a linear unmixing algorithm for depth and bottom retrieval, described in Section IV. The retrieval algorithm accounts for water surface reflections and variable bottom brightness and can be readily extended to include blends of different bottom materials.

The present work has similarities to as well as differences from previous remote bathymetry approaches. Sandidge and Holyer [1] cite a number of bathymetry algorithms that have been developed since the 1960s for multispectral sensors, including Landsat Thematic Mapper, and they present a new neural net-based method for hyperspectral imagery. Their method requires an extensive training set of spectra with known depths and a variety of bottom spectra, which may be provided from either measurements or simulations. Lee *et al.* [2] developed a first-principles bathymetry algorithm for hyperspectral data that uses parameterized simulations from Hydrolight [3], and applied it to an AVIRIS image of shallow water (0–4-m depth) with good success. In their method, atmospherically corrected (or "compensated") data are least squares fit to simulations using a five-dimensional nonlinear optimization algorithm in which depth, bottom brightness, and water properties (gelbstoff, turbid scattering, and phytoplankton) are varied. Most recently, Wozencraft *et al.* [4] analyzed Kaneohe Bay data from LASH and SHOALS using a semiempirical algorithm applicable to a fully illuminated sand bottom. Their algorithm requires some known depths and loses accuracy when shadows are present.

Manuscript received March 30, 2004; revised October 13, 2004. This work was supported by the National Geospatial-Intelligence Agency (NGA) SBIR Phase II Program under Contract NMA 201-01-C-0018. The NGA (formerly known as NIMA) does not necessarily endorse any opinions, conclusions, and views expressed in this paper.

S. M. Adler-Golden, P. K. Acharya, A. Berk, and M. W. Matthew are with Spectral Sciences, Inc., Burlington, MA 01803-3304 USA (e-mail: sag@spectral.com).

D. Gorodetzky is with Research Systems, Inc. Boulder, CO 80301 USA.

Digital Object Identifier 10.1109/TGRS.2004.841246

Our present algorithm most closely resembles that of Lee *et al.* [2]. It uses atmospherically corrected data, retrieves bottom brightness as well as depth, is physics-based, and is general enough to be applicable to many different types of imaging sensors. However, it makes the simplifying assumption of constant water optical properties within the scene. This avoids some ambiguities in separating the effects of different depths, bottom materials, and water types (e.g., turbid water scattering is difficult to distinguish from a shallower bottom.) In addition, this simplification improves the computational speed by an order of magnitude and allows the algorithm to be applied to four-channel MSI data, such as from QuickBird and IKONOS, as well as to HSI data. The algorithm also corrects for spectrally flat reflections from surface glint, foam, and thin clouds by taking advantage of one or more infrared channels, even when there is some contamination from water-leaving radiance. As part of this research, we investigated the problem of obtaining an accurate atmospheric correction in the LZ when ground truth reflectances are unavailable, and developed some improved methods for treating aerosol effects as well as a somewhat more accurate parameterization of water-leaving reflectance.

II. Atmospheric Correction

A. Overview

Atmospheric correction transforms measured radiance spectra into surface reflectance spectra. First-principles atmospheric correction typically consists of three steps. The first is the retrieval of atmospheric parameters, most notably an aerosol description (the visibility or optical depth, and, if possible, an aerosol "type") and the column water amount. Current methods allow aerosol retrieval over a very limited set of surface types (deep clear water and dark land); most often, retrieval of only a scene-average visibility is attempted. On the other hand, the spectral signature of water vapor is sufficiently distinct that the column amount may be retrieved on a pixel-by-pixel basis. The second step in the correction is the solution of the radiation transport (RT) equation for the given aerosol and column water vapor and transformation to reflectance. Finally, an optional postprocessing step called spectral polishing [5], [6] has been shown to remove many artifacts remaining after the physics-based correction is complete.

This section outlines the implementation of the first two steps in the Fast Line-of-sight Atmospheric Analysis of Spectral Hypercubes (FLAASH) atmospheric correction algorithm [7], [8] which we used to process the LZ data. FLAASH has been developed collaboratively by Spectral Sciences, Inc., the Air Force Research Laboratory, other U.S. government agencies, and Research Systems, Inc. (RSI). A commercial version of FLAASH is available from RSI as part of their ENVI software package.

B. Radiance Equation

The FLAASH atmospheric correction is based on a standard RT equation for spectral radiance at a sensor pixel L^* in the solar wavelength range (neglecting thermal emission) from a flat Lambertian surface or its equivalent [9]. Collecting constants reduces the equation to the form

$$L^* = a\rho/(1-\rho_e s) + b\rho_e/(1-\rho_e s) + L_a^*. \tag{1}$$

Here, ρ is the pixel surface reflectance, ρ_e is a surface reflectance averaged over the pixel and a surrounding region, s is the spherical albedo of the atmosphere, L_a^* is the radiance backscattered by the atmosphere, and a and b are coefficients that depend on atmospheric and geometric conditions but not on the surface. Each of these variables depends on the spectral channel; the wavelength index has been omitted for simplicity. The first term on the right-hand side of (1) is the radiance reflected from the surface that travels directly into the sensor. The second term is the radiance reflected from the surface that is scattered by the atmosphere into the sensor, resulting in a spatial blending, or adjacency effect [10]. Both FLAASH and the ATCOR code [11] solve the full (1) and thus account for this effect. However, many other atmospheric correction codes (e.g., ACORN [12], HATCH [13]) represent ρ and ρ_e by the same variable, resulting in neglect of the adjacency effect. This approximation, which is an option in FLAASH, is satisfactory for homogeneous surface areas, such as open ocean, and under high-visibility conditions, but it becomes inaccurate under hazy conditions in the LZ [7].

C. Radiation Transport Calculations

The three atmospheric constants in (1), a, b, and s are calculated from three Moderate Resolution Transmittance (MODTRAN) [14] radiance calculations with $\rho = 0.0, 0.5$, and 1.0. These calculations usually represent the single most computationally intensive part of the atmospheric correction. FLAASH performs a custom RT calculation for the image at hand to permit coverage of a wide range of conditions (e.g., off-nadir viewing, all MODTRAN standard aerosol models).

For the most accurate short-wave correction, the MODTRAN radiance calculations should be performed with the discrete-ordinate-method radiative transfer (DISORT) [15] multiple-scattering option rather than the computationally much faster two-stream method [16]. For a visibility of 25 km, the difference in calculated radiance between the two methods translates into a reflectance difference of roughly 0.01 at 500 nm. We have recently developed a new option in MODTRAN dubbed "DISORT scaling," which provides near-DISORT accuracy with almost the same speed as the two-stream method. In the DISORT scaling option, DISORT and two-stream calculations are performed at a small number of window region wavelengths. The multiple-scattering contributions in each method are identified and ratios of the DISORT and two-stream methods are computed. This ratio is interpolated over the full wavelength range, and finally applied as a multiple-scattering scale factor in a spectral radiance calculation performed with the two-stream method. In LZ applications, we have found that this procedure yields near-DISORT accuracy at window wavelengths, and also improves the accuracy in absorbing regions.

D. Atmospheric Parameter Retrieval

The values of a, b, s, and L_a^* in (1) depend on the viewing and solar angles and surface and sensor elevations, as well as on the atmospheric parameters of column water vapor, aerosol type, and visibility. Several methods have been developed for retrieving column water vapor using absorption bands. FLAASH uses the combination of an in-band/out-of-band radiance ratio and an out-of-band radiance to interrogate a MODTRAN-generated two-dimensional lookup table (LUT) for the column water vapor in each pixel. The water absorption band typically used is at 1.13 μm, with the LUT for this spectral region generated on-the-fly. With multispectral data or hyperspectral data having limited wavelength coverage, a different band may be needed for water retrieval, or no retrieval may be possible.

In water scenes, accurate retrieval and compensation of the aerosol or haze backscattering is critical for reliable results. Several methods have been developed for retrieving visibility, which defines the aerosol optical depth. If dark land pixels (2200-nm reflectance $< \sim 0.1$) are present, one may use FLAASH's adjacency-corrected implementation [8] of the Kaufman *et al.* [17] method, which is based on an empirical value (~ 0.5) of the 660–2200-nm reflectance ratio, for such pixels. We have recently adapted this algorithm to retrieve a scene-average visibility from water pixels. This was done by changing the dark pixel definition to select water (2200-nm reflectance $< \sim 0.015$) and, recognizing the spectral flatness of water surface reflectance in the infrared, by selecting a value of 1.0 for the reflectance ratio for a pair of channels beyond 900 nm, such as at 1000 and 2200 nm. With LZ scenes, both the land and water pixel methods may be used and the results checked for consistency.

A method for retrieving both visibility and aerosol "type" from deep water pixels in hyperspectral data has been developed by Gao *et al.* [18]. The aerosol type corresponds to a specific distribution of particle size and composition and thus has characteristic wavelength dependence. In their method, a given type is selected, a visibility is derived that generates the best fit to a flat spectrum at a set of infrared "window" wavelengths, and finally the "best" aerosol type and visibility are selected from among those results. This method can potentially retrieve visibility on a pixel-by-pixel basis; however, it was not designed to account for the adjacency effect.

As part of the current study, we have developed a related water-pixel method for FLAASH that retrieves a scene-average aerosol type with proper treatment of the adjacency effect. The details will be described in a future publication. In brief, the aerosol "type" is defined by a parameter (ΔN) that modifies the wavelength dependence of a chosen MODTRAN aerosol model (rural, maritime, etc.) via

$$E(\lambda) = E_0(\lambda)(550\,\text{nm}/\lambda)^{\Delta N}. \tag{2}$$

Here, E_0 is the unperturbed aerosol extinction coefficient, based on the chosen model's optical depth, which is uniformly scaled for all wavelengths λ according to the visibility parameter. The parameter ΔN changes the slope of the logarithm of the extinction curve. The scattering albedo and phase function of the modified aerosol are taken to be those of the unmodified model aerosol. Following Gao *et al.* [18], the retrieval algorithm works with a set of infrared window bandpasses, using the presumed wavelength dependence of the aerosol [i.e., (2)] to extrapolate the optical depth to the visible region. The infrared bandpasses are provisionally chosen as 2250 ± 40 nm, 1615 ± 70 nm, 1250 ± 20 nm, and 1050 ± 50 nm. For the average deep water radiance spectrum in these bandpasses, the algorithm finds the combination of ΔN and visibility that most closely fits a flat (but not necessarily zero) reflectance spectrum. It is assumed that extrapolation of the aerosol optical depth to shorter wavelengths is proper, as is also assumed by Gao *et al.* [18]. Our validation of this algorithm has been very limited to date; however, successful results were obtained with the AVIRIS image discussed in Section V. The new aerosol parameterization with ΔN has been added to our latest research version of MODTRAN.

All of the above aerosol retrieval algorithms rely on identifying and removing backscattered atmospheric radiance. Images taken from a very low altitude platform (within $\sim$1 km of the surface) may provide insufficient backscattering for accurate aerosol retrieval. On one hand, such images are correspondingly less sensitive to the aerosol amount, at least for dark surfaces such as water. On the other hand, bright surfaces such as sand remain sensitive to the aerosol amount via its effect on transmittance.

E. Solution of the Radiance Equation

Once the atmosphere is adequately characterized and the constants from (1) are derived, calculation of the image reflectance is straightforward using a method described elsewhere [7], [9]. It involves computing a spatially averaged radiance image L_e^*, from which the spatially averaged reflectance ρ_e is estimated using an approximation derived from (1)

$$L_e^* \approx (a+b)\rho_e/(1-\rho_e s) + L_a^*. \tag{3}$$

The spatial averaging is performed using a point-spread function that describes the relative contributions to the pixel radiance from points on the ground at different distances from the direct line of sight. FLAASH approximates this function as a nearly exponential function of radial distance. Since clouds can be a severe contaminant in the spatial averaging process for the L_e^* calculation, FLAASH automatically identifies cloudy pixels and replaces them with an average radiance.

F. Postprocessing

Even with the most accurate atmospheric correction, the reflectance results are susceptible to errors in the radiometric calibration of the sensor. Several investigators have reported radiometric offset errors in the blue region of the AVIRIS sensor [18], [19] that introduce reflectance errors as large as several hundredths. We found similar problems in the AVIRIS Tampa Bay and QuickBird images discussed later. Mustard and Prell [19] dealt with radiometric error in an AVIRIS image by abandoning first-principles atmospheric correction in favor of an "empirical line method" reflectance determination that used clouds and cloud shadows over water as, respectively, white (1.00 reflectance) and black (0.00 reflectance) "known" surfaces. This approach has its own problems, however. Clouds have variable brightness and unknown water vapor absorption, and in cloud shadows there can be reduced aerosol backscattering, which would result in under-subtraction of atmospheric scattered radiance elsewhere in the scene. Furthermore, many images contain no clouds.

In the current work, we treated radiometric errors by applying a simple offset to the FLAASH corrected images, derived from the minimum reflectance values for each spectral channel in the image. That is, we assumed that those minimum values correspond to zero reflectances occurring somewhere in these large and diverse scenes. At different wavelengths the minimum-reflectance pixels tend to originate from different types of surfaces, including deep water, cloud shadows over water, underwater vegetation, and land vegetation in shadow. This method has several potential problems, including the cloud shadow problem mentioned above. The minimum reflectance may remain above zero in the green region, even with both dark vegetation and deep water in the scene. A possible remedy is to interpolate the baseline between the red and blue regions, where it is likely that there are near-zero reflectance pixels. Another potential problem is the presence of "bad" pixels with artificially low reflectance, which must be excluded. However, based on the consistency of results that we obtained using different parts of the images, we estimated that the offset corrections were accurate to within several thousandths of a reflectance unit, and thus provided a substantial improvement to the FLAASH outputs.

III. Water-Leaving Reflectance Simulations

A. Calculation Method

Optical remote bathymetry requires representations of the water-leaving reflectance spectrum as a function of depth for realistic bottom materials and water composition. The Hydrolight code [3], [20] has been typically used for spectral simulations. We have adapted a three-dimensional direct simulation Monte Carlo (DSMC) radiation transport algorithm to perform these calculations. Details of the code are described elsewhere [21]. Standard extinction curves for pure water, chlorophyll and gelbstoff are used along with the Petzold [22] phase function for mineral scattering. The original motivation for developing and using the DSMC code was to treat three-dimensional spatial effects, associated with underwater objects and surface waves, as well as optical interaction between the water and the atmosphere. The simulations conducted for the present study did not require all these capabilities. We have verified that for the one-dimensional water cases compiled by Mobley *et al.* [20] the DSMC code gives equivalent results to Hydrolight.

B. Parameterization

Rather than performing spectral simulations with realistic underwater materials, we ran the simulations analogously to the MODTRAN calculations for FLAASH—that is, using spectrally flat surfaces—in order to develop empirical parameters for representing the spectra of arbitrary materials. The parameterization is based on an underwater analogue of (1) which, for simplicity, neglects the adjacency effect

$$R = A + R_g + B\rho/(1 - S\rho). \tag{4}$$

Here, A, B, and S are spectral parameters dependent on water composition and depth but independent of the bottom reflectance spectrum ρ. In contrast to (1), here the solar function and atmosphere have been removed. Thus, this equation represents water reflectance rather than radiance. The sum $A + R_g$ represents the scattered signal from photons that never reach the bottom; this consists of the combined surface Fresnel reflection and foam spectral component R_g (we represent this as a flat spectrum) and the subsurface scattering component A. S, which corresponds to the atmospheric spherical albedo in the atmospheric correction problem, here represents the probability that a photon leaving the bottom returns to it; it includes water–air interface reflection, water scattering, and absorption effects. The derivation of (4) follows that of the atmospheric case, since analogous physical phenomena are present. For monochromatic radiation, the equation remains valid for arbitrary quantities of absorbing or scattering materials in the water. For a given depth d and water type, the three spectral unknowns A, B, and S are determined by solving (4) using three different DSMC simulations of the R spectrum, corresponding to $\rho = 0, 0.5$, and 1.

A different parameterization of water reflectance has been proposed [23] based on "subsurface reflectance" $R_{\rm sub}$ defined by the equation

$$R = \frac{0.52\, R_{\rm sub}}{1 - 0.48\, R_{\rm sub}} \tag{5}$$

where $R_{\rm sub}$ is taken as linear in ρ. However, a careful analysis of our DSMC simulations revealed a small sublinear dependence of $R_{\rm sub}$ on ρ. We ascribe this effect to absorption-induced non-Lambertian behavior of the subsurface radiation field. Specifically, illumination of the bottom by internally reflected radiation is reduced relative to direct solar illumination because the internally reflected rays, which are at less vertical angles, are more strongly absorbed by the water. For these reasons, we believe that the parameterization given by (4) is preferable to (5).

For an efficient bathymetry algorithm, analytical representations of A, B, and S in terms of depth d are desired. Motivated by Lee *et al.* [23] and others who express $R_{\rm sub}$ using parameters that depend exponentially on d, we tried exponential forms for A, B, and S

$$A = A_{\rm inf}[1 - \exp(-k_a d)] \tag{6}$$

$$B = 0.52\exp(-k_b d) \tag{7}$$

$$S = 0.48\exp(-k_s d). \tag{8}$$

The k values depend on the wavelength and water composition. We found these equations to represent the DSMC simulations very well for monochromatic wavelengths or narrow ($\sim$10 nm) hyperspectral channels. However, for wide multispectral bandpasses we found that the B parameter, which is the most important of the three, deviates significantly from exponential behavior. Therefore, we allow a depth-dependence in k_b by log-interpolating B between the simulation depths.

C. Simulation Database

For use with our bathymetry algorithm, an extensive database, or "library," of DSMC-simulated reflectance spectra was assembled. The $\rho = 0, 0.5$, and 1 spectra were calculated between $\sim$390 and 800-nm at $\sim$10-nm intervals for a series of nine water depths (1, 3, 5, 10, 15, 20, 30, 40, and 50 m), 64 different combinations of gelbstoff, chlorophyll and turbidity levels (designated None, Low, Medium, High), and three different solar zenith angles (15, 40, and 60°), for a total of 5184 library spectra. The Low, Medium, and High chlorophyll levels corresponded to, respectively, 0.5, 1.0, and 2.0 times the Celtic Sea profile in Mobley *et al.* [20]. The low, medium, and high levels for gelbstoff and turbidity are based on Lee *et al.* [23] and correspond to, respectively, three different levels of 440-nm extinction (0.05, 0.1, and 0.3 per meter) and three different values (0.3, 1.0, and 5.0) of the profile factor B in their paper. The Low gelbstoff, Low turbidity, and Medium chlorophyll model is designated the "baseline ocean" case.

IV. Bathymetry Algorithm Description

A. Water Depth and Surface Reflection Determination

Once A, B, and S [(6)–(8)] have been determined from the DSMC calculations and the water reflectance R derived by atmospherically correcting the radiance image, (4) can be solved for the bottom reflectance spectrum ρ

$$\rho = (R - A - R_g)/[B + S(R - A - R_g)]. \tag{9}$$

The result depends parametrically on the water depth. We assume that the R_g spectrum can be expressed as the product of a fixed spectral shape s_g (typically taken as flat) and a magnitude g. g may be inferred from infrared wavelengths beyond ~750 nm, where light from below the surface can be neglected. Then we may use linear spectral unmixing to represent ρ as a combination of bottom material "basis" spectra for each possible depth, and then assign the true depth as that which gives the best fit. With multiple spectrally distinguishable materials, the unmixing should be constrained to have nonnegative weights that sum to unity or less, to account for possible shadowing. Currently we use only a single bottom material, taken from a dry shoreline (i.e., sand) pixel, with a variable weight to account for shadowing and brightness variations.

With some sensors, even the longest wavelength channel can be contaminated with light from below the water surface, especially in very shallow water (<1-m deep). In this case, the magnitude g of the water surface spectrum cannot be determined as described above. Accordingly, we have extended the multiple-material unmixing method to allow its retrieval. This is done by linearizing (9) with respect to R_g so that the surface reflectance can be treated as an effective additive bottom component G. A Taylor series expansion around $R_g = 0$ yields the result

$$\rho = (R - A)/[B + S(R - A)] - G \tag{10}$$

where

$$G = BR_g/[B+S(R-A)]^2 = gBs_g/[B+S(R-A)]^2. \tag{11}$$

Note that in (10), the quantity $(R - A)/[B + (R - A)]$, which combines both the measured water-leaving reflectance and the simulation model parameters, is expressed as the sum of G and the bottom reflectance. We have verified that this linearized equation agrees very closely with the exact (9) for physically reasonable R_g values (of order 0.1 or less).

A drawback of performing the unmixing on the quantity $\rho+G$ is that it weights the R measurement error very unevenly with respect to wavelength. For the typical case where $S(R-A) \ll B, G$ is approximately R_g/B and $(R-A)/[B+S(R-A)]$ is approximately $(R-A)/B$, so the error has a $\sim 1/B$ weighting, giving it a strong boost at absorbing wavelengths where B is very small. A simple way to get around this problem is to scale the quantities $(R - A)/[B + S(R - A)], G$ and ρ by B and perform the linear unmixing on the results.

A simultaneous bathymetry, bottom material unmixing and surface reflection removal procedure can now be devised as follows.

Step 1) For a selected water depth, using an appropriate (e.g., spectrally flat) surface reflectance spectral shape s_g, the A, B, and S parameters of the water model simulation, and the measured water-leaving reflectance spectrum R, form the scaled surface spectrum Bs_g and the scaled total reflectance $y = B(R - A)/[B + S(R - A)]$.

Step 2) Form synthetic $B\rho$ spectra for one or more bottom material reflectance spectrum components ρ_i. These will be used to form the spectral quantity

$$B\rho = \sum_i W_i B\rho_i \tag{12}$$

where the W_i are to-be-determined abundances, or weights, for each material.

Step 3) The working equation is now

$$y = gBs_g + \sum_i W_i B\rho_i + \text{error} \tag{13}$$

with g and the W_i as unknown coefficients and y, Bs_g, and $B\rho_i$ as known spectral components. Determine the coefficients *via* a linear spectral fitting procedure that minimizes the RMS error spectrum (this is the "unmixing" step). To avoid unphysical solutions, include at least a positivity constraint on the coefficients. An efficient method based on modified Gram–Schmidt orthogonalization is described by Gruninger *et al.* [24].

Step 4) Repeat Steps 2) and 3) over a range of water depths, and select the unmixing solution that gives the smallest RMS error. The depths covered in the present work range from 0–19 m.

B. Water Constituents Estimation Using "Known" Depths

The shape of the reflectance spectrum and hence the A, B and S parameters depend on the water constituents, especially as the depth increases. Taking advantage of this, Lee *et al.* [2] report retrieval of water constituents by direct hyperspectral data fitting using "known" bottom material spectra. However, multispectral data, typically with only four channels, lack sufficient information for such retrievals, and even with hyperspectral data some ambiguities in the retrievals are expected. For example, turbidity can produce spectral changes similar to a decrease in depth with a fairly spectrally flat bottom material such as sand. Gelbstoff reduces the blue reflectance, but might be confused with the presence of a more yellowish bottom material. Accordingly, we have developed a procedure for estimating water constituents from pixels where the depth is known, or where the water is known to be much deeper than the desired range of depths to be retrieved.

In this procedure, the previously described bathymetry algorithm is used, with the surface reflection and bottom brightness allowed to vary but the depth fixed. The best fit spectrum is reported and compared with the data for each trial water model. From such comparisons we were able to find an unambiguous "best" model from among the 64 water types in our spectral library for the AVIRIS and LASH data discussed here as well as for a Hyperion image of the Virgin Islands [25]. An alternative procedure is to perform bathymetry retrievals with different water models and select the best model from comparisons with known depths. If the pure water model is used, the retrieved depths may be underestimated due to the presence of turbidity. We observed this effect with an AVIRIS image of Chesapeake Bay, where the maximum retrieved depth was only a few meters. For that case, a more turbid water model should yield more realistic depths; however, the inherent lack of depth sensitivity of the spectrum would remain a problem.

We expect that little or no information on water constituents will be obtainable from multispectral data, such as from Landsat, QuickBird or IKONOS, that have only three bands in the visible. This is because in water more than a few meters deep, the red water-leaving radiance is completely absorbed, leaving only two wavelength measurements (blue and green) from which one must determine the bottom brightness and at most one other parameter. If the bottom brightness is assumed to be known, some constituent information should in principle be retrievable, but then the bathymetry results are sensitive to variations in illumination (e.g., shadows) [4].

V. Data Analysis

A. LASH Imagery of Kaneohe Bay

A set of images of Kaneohe Bay, Hawaii was acquired by the Laser Airborne Sensor—Hyperspectral (LASH) sensor (STI Government Systems, Honolulu) in April, 2002 under a program sponsored by the National Imagery and Mapping Agency [currently the National Geospatial-Intelligence Agency (NGA)]; the data were kindly provided to us by STI. Thirteen tracks (data strips) of imagery were taken with LASH's two nadir-viewing hyperspectral cameras, which are designated Camera 0 and Camera 1. The instrument was flying about 800-m above the water, yielding a pixel size of around 1 m. The spectra cover approximately the 390–730-nm range, with a width and spacing of ~7 nm defined by the binning of multiple spectral columns of the focal plane. We adjusted the supplied wavelength calibration as needed for consistency with MODTRAN spectral radiance calculations as well as other HSI data. The LASH images are accompanied by georeferencing data with a reported horizontal accuracy of about 30 m.

Overlapping bathymetry data were provided from a Scanning Hydrographic Operational Airborne Lidar Survey (SHOALS) (Optech International, Inc., Stennis Space Center, MS) data collect in August, 2000. The SHOALS system measures water depth down to around 50-m at a horizontal grid density of around 4 m. These data were supplied in easting-northing

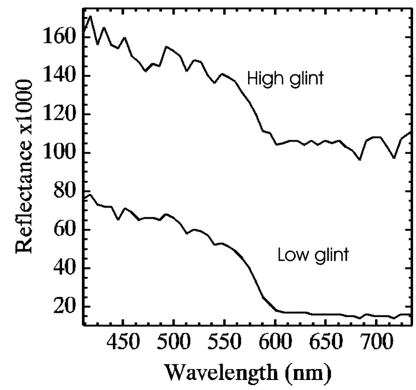

Fig. 1. Comparison of LASH spectra at similar depths with different amounts of glint.

coordinates on an irregular grid, which was converted to longitude-latitude and interpolated to the LASH pixel coordinates.

The limited IR coverage of the LASH data made it difficult to extract parameters for the atmospheric correction, particularly for the aerosol. However, the needed aerosol correction is modest because the sensor was close to the water surface. We assumed the MODTRAN maritime aerosol model. Using the corrected wavelengths an atmospheric water vapor column density of ~3.3 g/cm^2 was retrieved from the 720-nm band and ~20-km visibility from land vegetation pixels. Finally, a small offset spectrum derived as described in Section VI was applied.

As the Kaneohe Bay water is known to be very clear, we began the bathymetry retrieval with the pure water model. Both gelbstoff and turbidity tend to mask the characteristic water absorption features and make the spectra look more like those of bottom materials; therefore, significant quantities of these impurities would be expected to result in underestimated water depths with this model. To reduce the sensitivity of the retrieval to gelbstoff concentration, the wavelength region used for retrieval was restricted to greater than 525 nm.

As the sun was high (15° zenith angle) during the measurements, a large amount of glint from surface waves, up to around 20% reflectance, was found in many pixels. Example spectra from Track 1 Camera 0 are shown in Fig. 1; here the top spectrum has a spectrally flat glint offset of around 10% reflectance. Except in the deepest water, where the signal from below the surface is very small, the glint was subtracted well enough to retrieve an accurate subsurface spectrum. This is shown in the Fig. 2 images of a small part of the data strip where the water is 4–8-m deep. Even though the original reflectance image is overwhelmed by glint, the glint-removed image is free from wave clutter and reveals the underwater environment. The ocean bottom image is similar to the glint-removed image; in a color rendition it appears light brown, appropriate for a coral sand bottom.

The bathymetry results for Track 1 Camera 0 are compared against the SHOALS ground truth depths in the Fig. 3 scatter plot and Fig. 4 histogram plot. The comparisons were performed with a ~100-m shift between the LASH and SHOALS images to correct for a geographic misregistration, which was evident from the depth maps. The mean systematic error in the depth retrievals is around −25%, and the half-width of the distribution

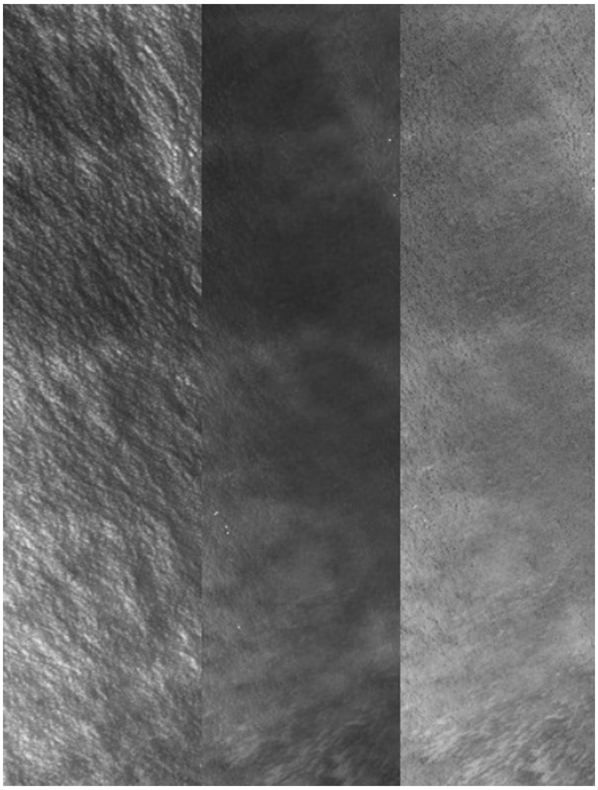

Fig. 2. LASH images of 4–8-m deep water in Track 1 Camera 0. At left, original reflectance image after atmospheric correction. At center, image after glint removal. At right, retrieved image of ocean bottom.

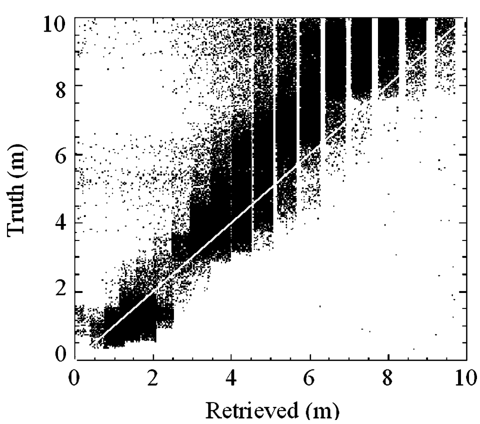

Fig. 3. Scatter plot comparison of retrieved and SHOALS truth bathymetry for LASH Track 1 Camera 0. Retrieval assumed the pure water model. White diagonal line corresponds to perfect agreement.

around the mean is 1.0–1.5 m. The direction of the systematic error is consistent with expectations for the pure water model, as discussed above. The striping of the scatter plot originates from the discrete gridding of the retrieved values. To reduce the overlap of data points and thereby improve the appearance of the plot, a small amount of random noise has been added to the retrieved values.

Results for a portion of Track 3 Camera 0 are shown in Fig. 5. Coral structures are prominent in the bottom image and the depth map, and allow the data to be georegistered with the SHOALS bathymetry to within a few meters. The level of agreement between the true and retrieved depth is similar to that in Track 1 Camera 0.

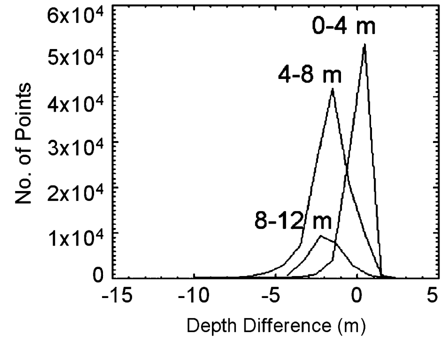

Fig. 4. One-meter histogram comparison of the Fig. 3 data.

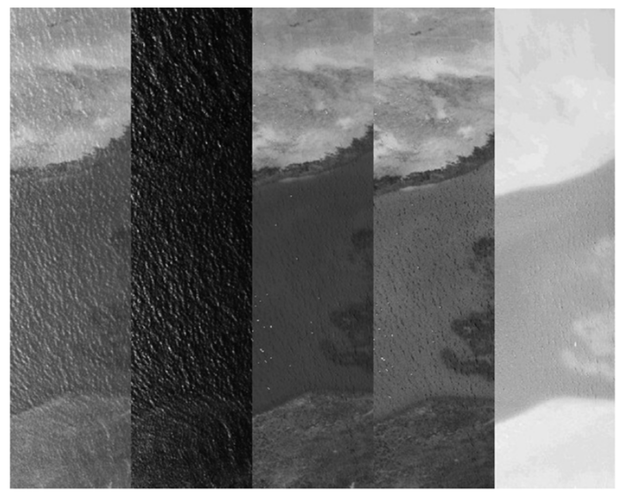

Fig. 5. Results from a shallow water portion of LASH Track 3 Camera 0 showing coral features. From left, original image, surface glint, glint removed, bottom, and depth.

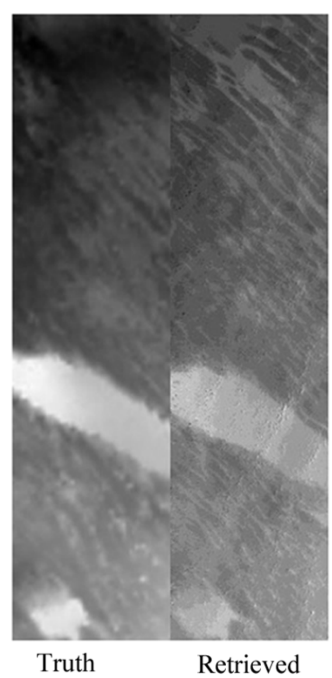

Fig. 6. Grayscale depth map comparison for LASH Track 3 Camera 0.

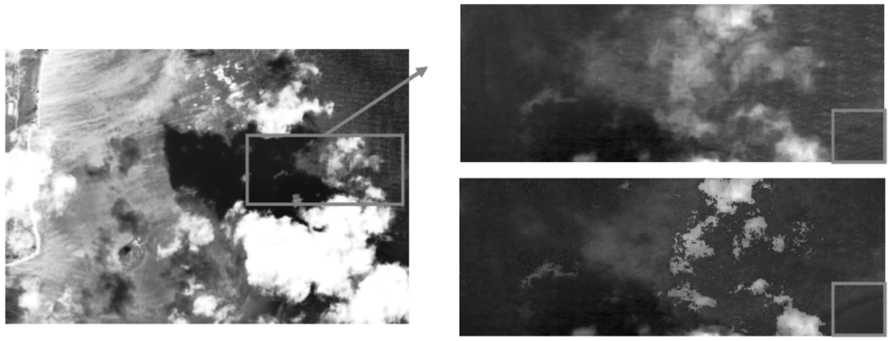

(a) (b)

Fig. 7. Detail of a $\sim 0.5 \times 1.25$ km analyzed region of the QuickBird image of Kaneohe Bay. The lower image at right has surface reflection and thin clouds removed. Small square at lower right indicates deep water beyond the edge of the reef.

The images in Fig. 2 show some dark patches where the glint and bottom brightness are correlated. We interpret these patches as thin cloud shadows. Later in this section we present QuickBird imagery that contains numerous cloud shadows, including nearly opaque shadows from thick cumulus clouds. Because our bathymetry algorithm accounts for variable bottom brightness, it is rather insensitive to illumination variations arising from thin clouds as well as from wave-related lensing effects. However, if the shadows are very dark, the water-leaving radiance signal becomes too small to be separated from atmospheric backscattering, and the retrieval fails.

Fig. 6 shows a grayscale comparison of truth and LASH-retrieved bathymetry for a deeper portion of Track 3 Camera 0. The depths range from around 2 m (white) to around 8 m (black). This image shows the high spatial resolution of the depth retrieval, which is equal to or better than that of the SHOALS ground truth data. The retrieval accuracy is similar to that shown in Figs. 3 and 4.

Improvements upon the current LASH bathymetry results might be obtained by using a more accurate water description, perhaps one intermediate between the pure water and Low gelbstoff models in our library. In combination with this, the retrieval wavelength range could be extended to $\sim$500 nm or lower, as was done in our subsequent analysis of QuickBird data of Kaneohe Bay, described next.

B. QuickBird Imagery of Kaneohe Bay

Imagery of Kaneohe Bay was acquired by the QuickBird satellite sensor on February 20, 2002, two months before the LASH data collect. The pixel size is around 2.6 m. We obtained a 42-km^2 subset of the archived data (DigitalGlobe Cat. ID 1010010000206701, http://www.digitalglobe.com), and analyzed several portions of it. The portion shown in Fig. 7 overlaps the SHOALS bathymetry and is largely free of thick clouds, although much of it is in cloud shadow.

A FLAASH atmospheric correction with a default visibility (40 km) generated realistic spectra; shadows on both land and water have close to zero reflectance, and bright clouds have a spectrally flat reflectance of around 0.6. This gives us confidence that the radiometric calibration of QuickBird and the aerosol loading estimate are reasonably accurate. The reflectances were refined by applying a small offset using the method described in Section II-F. As in the LASH data analysis, the pure water model was assumed for the bathymetry retrieval.

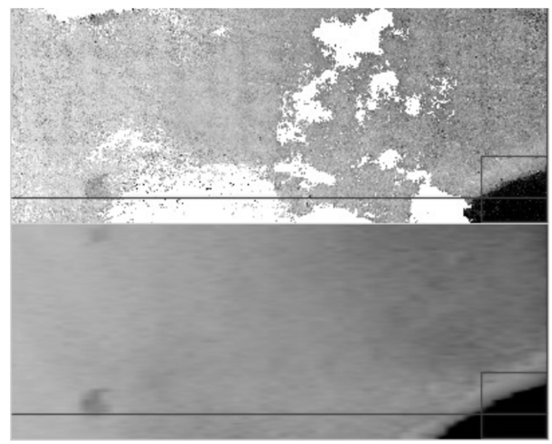

Fig. 8. Grayscale depth maps for the Fig. 7 QuickBird image. Top image shows the retrieved depths, with cloud- and shadow-masked areas in white; bottom image shows the SHOALS ground truth.

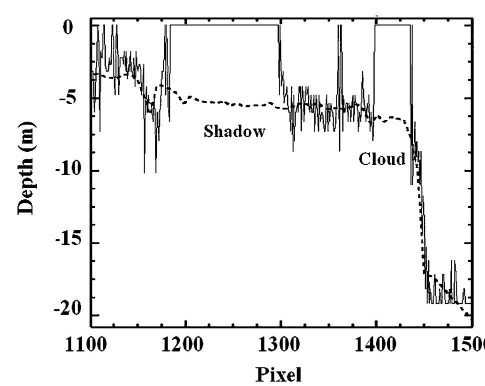

Fig. 9. Comparison of QuickBird retrieved (solid curve) and SHOALS truth (dashed curve) depths along the horizontal line in Fig. 8. Retrieved values are set to zero in cloud- and shadow-masked pixels.

The bathymetry algorithm masks out land, thick clouds, and deep shadow and attempts retrievals for the remaining pixels. Thin clouds are treated like surface reflections and are removed, as seen in the Fig. 7 detail region. Depth results for that region are displayed in Figs. 8 and 9. The overall agreement between the retrieved and true depths is seen to be quite reasonable, particularly in the fully illuminated areas outside the cloud

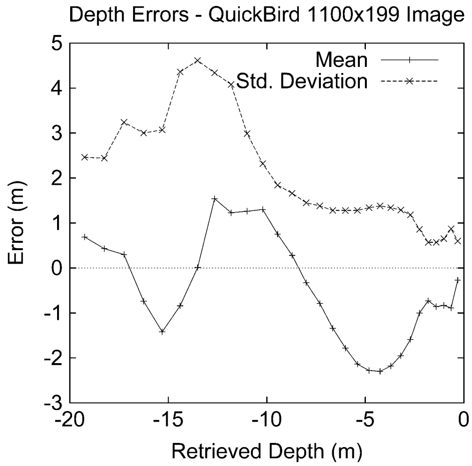

Fig. 10. Depth retrieval error statistics as a function of depth for a strip of the Fig. 7(left) QuickBird image.

shadows, and including the patch of relatively deep (~20 m) water at the lower right. The typical error is around 1 m; most of it appears to be a random pixel-to-pixel variation, which we ascribe to radiance measurement noise.

More quantitative estimates of the depth retrieval accuracy were made for a 0.5-km-tall horizontal strip of Fig. 7(a) that starts from the shoreline and continues out to, and includes, the detail region; this strip contains approximately 160 000 usable water pixels. The results, in Fig. 10, are expressed in terms of the mean (systematic) error and the standard deviation about the mean (this measures the spread in retrieval errors) as a function of retrieved depth. For unknown reasons, the systematic error reaches a maximum of just over 2 m at around 6-m depth. However, over most of the 0–19-m range, it remains well below 2 m.

C. AVIRIS Image of Tampa Bay

Measurements of the Tampa Bay area were made by the AVIRIS hyperspectral sensor on May 21, 1999 from an altitude of 20 km. The pixel size is around 20 m. From the original data strip (f990521t01p02, available from the Jet Propulsion Laboratory, http://aviris.jpl.nasa.gov/), we prepared a 600 × 900 pixel image (Fig. 11) that is largely covered by NOS bathymetry from the 1940s and 1950s. The image was atmospherically corrected using FLAASH with several different aerosol retrieval methods. The different methods gave somewhat different results for the visibility. The method in Section II-D yielded $\Delta N = -1.0$ and a 45-km visibility using the MODTRAN rural aerosol model as the reference. The resulting modified wavelength dependence is very similar to that of the marine model, which we used for further analysis of the data. Following FLAASH processing, we derived and subtracted an estimated reflectance offset spectrum as described in Section II-F. The offset was 0.01 or less above 500 nm, where both the aerosol retrieval and bathymetry are performed, but at 430 nm it was very large (around 0.07).

The bathymetry algorithm was run on the reflectance image using the base ocean water model. The results are compared with the NOS data in Figs. 12 and 13. Due to the age of the NOS bathymetry, it is difficult to draw quantitative conclusions about the retrieval accuracy. However, in qualitative terms the agreement appears reasonable over most of the scene. The histograms in Fig. 13 indicate that for depths down to −10 m, the average difference is a little less than 1 m, and that there is agreement to within 2 m for nearly all pixels.

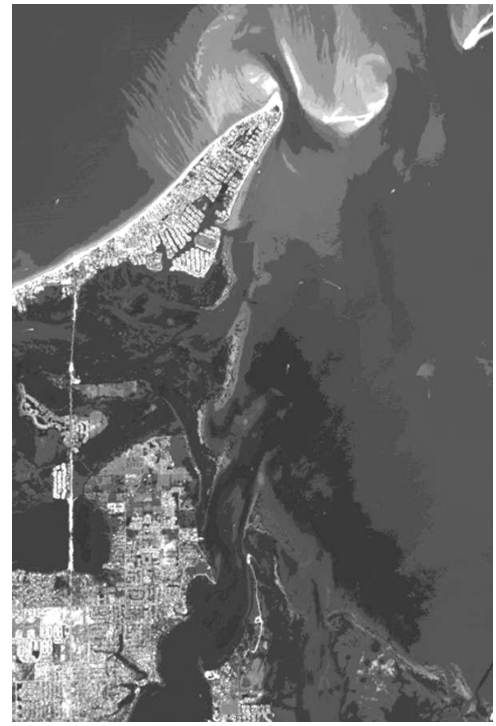

Fig. 11. AVIRIS radiance image of the south Tampa Bay area, May 21, 1999. Dimensions are $\sim 12 \times 18$ km.

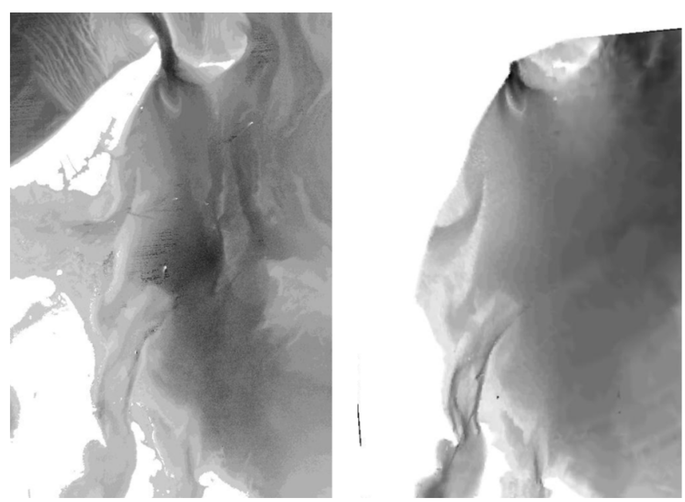

(a) (b)

Fig. 12. Grayscale maps of (a) retrieved and (b) NOS bathymetry for the AVIRIS Tampa Bay scene.

VI. Summary and Conclusion

This work has demonstrated the application of hyperspectral and multispectral remote imagery to remote bathymetry in the littoral zone using physics-based atmospheric correction and retrieval algorithms. The results include depth maps and bottom visualizations. As part of this effort, atmospheric correction in the littoral zone was advanced through new capabilities added

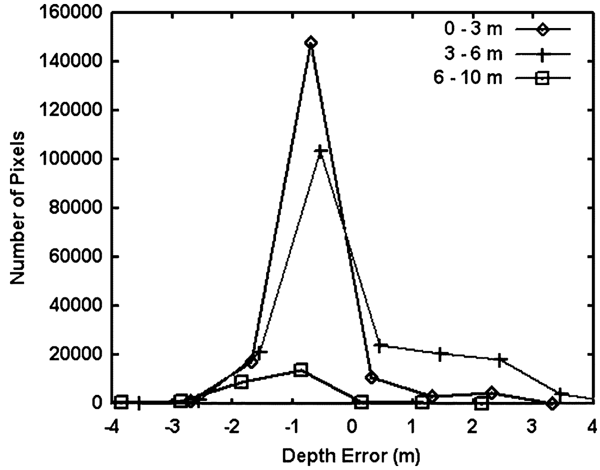

Fig. 13. Histogram comparison of the retrieved and NOS depths for Tampa Bay.

to the FLAASH atmospheric correction and MODTRAN radiation transport codes; these include improved characterization of the aerosol wavelength dependence and a DISORT scaling technique for rapidly calculating multiply scattered radiance in atmospheric window wavelength regions. The depth retrieval algorithm, which uses spectral reflectance data, accounts for water surface reflection and thin clouds, while simultaneously retrieving bottom brightness and depth. With a nearly overhead sun, glint contributions can be quite large (of order 0.1 reflectance), but they can usually be removed satisfactorily.

Analyses of AVIRIS, LASH, and QuickBird data have been undertaken, including imagery of Kaneohe Bay, HI, overlapping with laser bathymetry data. The depth retrieval accuracy, typically within a couple of meters from 0–10-m depths, is similar to what has been reported by other investigators [1], [2], [4] using different algorithms over littoral areas of comparable size and water clarity. The results are quite sensitive to the accuracy of the sensor radiometric calibration, the knowledge of the bottom material spectrum, and the ability to estimate the water optical properties. The maximum retrievable depth is limited by the turbidity of the water. In addition, we found that accurate bathymetry beyond several meters depth requires very high accuracy in the radiometric baseline, to within a few thousandths of a reflectance unit. For the data we studied, this generally necessitated applying an empirical baseline offset to the reflectance after a first principles atmospheric correction was performed. The depth retrievals were rather insensitive to partial shadow, such as from thin clouds; however, retrievals were not possible in thick cloud shadows due to a lack of signal.

With hyperspectral imagery under favorable conditions, such as when there is independent depth information or the bottom spectrum is well known, some water composition information can be inferred; in particular, the blue region of the spectrum is sensitive to the level of gelbstoff. However, with typical multispectral imagery we find that, in the presence of water surface reflections, only depth and bottom brightness are retrievable, since there are typically only three or four spectral channels containing independent information.

While the current algorithms work reasonably well with a variety of remote imagery, the work of Lee *et al.* [2] suggests that, at least with hyperspectral data, further improvements may allow additional information on the water and bottom composition to be retrieved. In addition, we recommend further work to optimize the selection of spectral channels for the analysis and to more accurately convert the water-leaving spectra to reflectance.

ACKNOWLEDGMENT

The authors are grateful to M. Topping and C. Leonard (STI Industries, Honolulu, HI) and F. Kruse (Analytical Imaging and Geophysics LLC) for providing data for analysis. Permission was obtained for all images analyzed in this paper.

REFERENCES

[1] J. C. Sandidge and R. J. Holyer, "Coastal bathymetry from hyperspectral observations of water radiance," *Remote Sens. Environ.*, vol. 65, pp. 341–352, 1998.

[2] Z. Lee, K. L. Carder, R. F. Chen, and T. G. Peacock, "Properties of the water column and bottom derived from Airborne Visible Imaging Spectrometer (AVIRIS) data," *J. Geophys. Res.*, vol. 106, pp. 11 639–11 651, 2001.

[3] C. D. Mobley and L. K. Sundman, *Hydrolight 4.1 User Guide*. Redmond, WA: Sequoia Scientific, 2000.

[4] J. Wozencraft, M. Lee, G. Tuell, and W. Philpot, "Use of SHOALS data to produce spectrally-derived depths in Kaneohe Bay, Hawaii," in *U.S. Hydrographic Conf.*, Biloxi, MS, Mar. 24–27, 2003.

[5] J. W. Boardman, "Post ATREM polishing of AVIRIS apparent reflectance data using EFFORT: A lesson in accuracy versus precision," in *Summaries of the 7th JPL Airborne Earth Science Workshop*, vol. 1, 1998, JPL Pub. 97-21, p. 53.

[6] S. M. Adler-Golden, M. W. Matthew, L. S. Bernstein, R. Y. Levine, A. Berk, S. C. Richtsmeier, P. K. Acharya, G. P. Anderson, G. Felde, J. Gardner, M. Hoke, L. S. Jeong, B. Pukall, A. Ratkowski, and H.-H. Burke, "Atmospheric correction for short-wave spectral imagery based on MODTRAN4," *Proc. SPIE*, vol. 3753, pp. 61–69, 1999.

[7] M. W. Matthew, S. M. Adler-Golden, A. Berk, G. Felde, G. P. Anderson, D. Gorodetzky, S. Paswaters, and M. Shippert, "Atmospheric correction of spectral imagery: Evaluation of the FLAASH algorithm with AVIRIS data," *Proc. SPIE*, vol. 5093, pp. 474–482, 2003.

[8] M. W. Matthew, S. M. Adler-Golden, A. Berk, S. C. Richtsmeier, R. Y. Levine, L. S. Bernstein, P. K. Acharya, G. P. Anderson, G. W. Felde, M. P. Hoke, A. Ratkowski, H.-H. Burke, R. D. Kaiser, and D. P. Miller, "Status of atmospheric correction using a MODTRAN4-based algorithm," *Proc. SPIE*, vol. 4049, pp. 199–207, 2000.

[9] E. F. Vermote, N. El Saleous, C. O. Justice, Y. J. Kaufman, J. L. Privette, L. Remer, J. C. Roger, and D. Tanré, "Atmospheric correction of visible to middle-infrared EOS-MODIS data over land surfaces: Background, operational algorithm and validation," *J. Geophys. Res.*, vol. 102, pp. 17 131–17 141, 1997.

[10] D. Tanré, M. Herman, and P. Y. Deschamps, "Influence of the background contribution upon space measurements of ground reflectance," *Appl. Opt.*, vol. 20, pp. 3676–3684, 1981.

[11] R. Richter, "Bandpass resampling effects on the retrieval of radiance and surface reflectance," *Appl. Opt.*, vol. 39, pp. 5001–5005, 2000.

[12] R. Green, "Atmospheric correction now (ACORN)," Analytical Imaging and Geophysics, Boulder, CO, 2001.

[13] A. Qu, B. C. Kindel, and A. F. H. Goetz, "The high accuracy atmospheric correction for hyperspectral data (HATCH) model," *IEEE Trans. Geosci. Remote Sens*, vol. 41, no. 6, pp. 1223–1231, Jun. 2003.

[14] A. Berk, L. S. Bernstein, P. K. Acharya, D. C. Robertson, S. M. Adler-Golden, G. P. Anderson, and J. H. Chetwynd, "MODTRAN cloud and multiple scattering upgrades with application to AVIRIS," *Remote Sens. Environ.*, vol. 65, pp. 367–375, 1998.

[15] K. Stamnes, S.-C. Tsay, W. Wiscombe, and K. Jayaweera, "Numerically stable algorithm for discrete-ordinate-method radiative transfer in multiple scattering and emitting layered media," *Appl. Opt.*, vol. 27, pp. 2502–2509, 1988.

[16] R. G. Isaacs, W. C. Wang, R. D. Worsham, and S. Goldenberg, "Multiple scattering LOWTRAN and FASCODE models," *Appl. Opt.*, vol. 26, pp. 1272–1281, 1987.

[17] Y. J. Kaufman, D. Tanré, L. A. Remer, E. F. Vermote, A. Chu, and B. N. Holben, "Operational remote sensing of tropospheric aerosol over land from EOS Moderate Imaging Spectroradiometer," *J. Geophys. Res.*, vol. 102, no. 17051, 1997.

[18] B.-C. Gao, M. J. Montes, Z. Ahmad, and C. O. Davis, "Atmospheric correction algorithm for hyperspectral remote sensing of ocean color from space," *Appl. Opt.*, vol. 39, pp. 887–896, 2000.
[19] J. F. Mustard and W. Prell, "Diverse spectral properties in a temperature estuary: First results from Narragansett Bay, Rhode Island," in *Summaries of the7th JPL Airborne Earth Science Workshop*, vol. 1, 1998, JPL Pub. 97-21.
[20] C. D. Mobley, B. Gentili, H. R. Gordon, Z. Jin, G. W. Katawar, A. Morel, P. Reinersman, K. Stamnes, and R. H. Stavn, "Comparison of numerical models for computing underwater light fields," *Appl. Opt.*, vol. 36, no. 7484, 1993.
[21] S. C. Richtsmeier, A. Berk, L. S. Bernstein, and S. M. Adler-Golden, "A 3-Dimensional radiative-transfer hyperspectral image simulator for algorithm validation," in *Proc. Int. Symp. Spectral Sensing Research (ISSSR)*, Quebec, ON, Canada, Jun. 2001.
[22] T. J. Petzold, "Volume scattering functions for selected ocean waters," Visibility Lab., Scripps Inst. Oceanography, San Diego, CA, SIO Ref. 72–78, 1972.
[23] Z. Lee, K. L. Carder, C. D. Mobley, R. G. Steward, and J. S. Patch, "Hyperspectral remote sensing for shallow waters. I. A semianalytical model," *Appl. Opt.*, vol. 37, pp. 6329–6338, 1998.
[24] J. Gruninger, M. J. Fox, and R. L. Sundberg, "Hyperspectral mixture analysis using constrained projections onto material subspaces," in *Proc. Int. Symp. Spectral Sensing Research (ISSR)*, Quebec, ON, Canada, Jun. 2001, pp. 11–15.
[25] F. A. Kruse, "Preliminary results—Hyperspectral mapping of coral reef systems using EO-1 Hyperion, Buck Island, U.S. Virgin Islands," in *Proc. 12th JPL Airborne Geoscience Workshop*. Pasadena, CA, Feb. 2003, pp. 24–28.

Steven M. Adler-Golden received the Ph.D. degree in physical chemistry from Cornell University, Ithaca, NY, in 1979, working under Prof. John Wiesenfeld.

He is currently the Leader of the Remote Sensing Group at Spectral Sciences, Inc., Burlington, MA. His experience at both the technical and management levels includes atmospheric aeronomy, infrared/visible/ultraviolet radiation modeling, and prototype trace gas sensor development. He has played leading roles in the development of atmospheric correction, data analysis, and data simulation algorithms for spectral imagery based on MODTRAN. His research background combines experimental work and modeling. He did postdoctoral work under Prof. Jeffrey Steinfeld at the Massachusetts Institute of Technology on ozone spectroscopy and energy transfer prior to joining Spectral Sciences in 1981.

Prabhat K. Acharya received the M.S. degree in computer science from the University of Utah, Salt Lake City, and the Ph.D. degree in chemical physics from the University of North Carolina, Chapel Hill, in 1982 and 1987, respectively.

He is currently a Principal Scientist with Spectral Sciences, Inc. (SSI), Burlington, MA. He has extensive experience in the areas of atmospheric radiance and transmission modeling and simulation. He has played a key technical role in the collaborative development by SSI and the Air Force Research Laboratory of the MODTRAN radiation transport code. He is currently engaged in developing very rapid techniques for modeling atmospheric radiance in broad bandpasses. He was a Postdoctoral Fellow with Prof. Jack Simons at the University of Utah, where he calculated rates and formulated propensity rules for electron autodetachment of vibrationally excited molecules. His M.S. work in computer science under the supervision of Profs. Thomas C. Henderson and Bir Bhanu involved applications and development of Hough transform and least squares techniques for range data analysis for computer vision applications. His Ph.D. work in chemistry under the supervision of Prof. Robert G. Parr was in the area of electron density functional theory.

Alexander Berk received the B.S. degrees in chemistry and mathematics from Harvey Mudd College, Claremont, CA, in 1978, and the Ph.D. degree from the University of North Carolina, Chapel Hill, in 1983.

He is currently a Principal Scientist and Special Project Director with Spectral Sciences, Inc., Burlington, MA, where he has served as technical and management leads on numerous modeling and code development projects in the area of radiation transport. His research has concentrated on atmospheric transmittance and radiance phenomena, including development of modules for the Air Force Research Laboratory's MODTRAN, SHARC, and SAMM radiation codes, calculation of infrared and ultraviolet radiation signatures from high- and moderate-altitude rocket fuel dumps, modeling of cloud clutter radiation in the MWIR and LWIR, and development of high-temperature band models His graduate research with Prof. Robert G. Parr centered on the development and application of techniques for calculation of lower bound molecular energies in Hartree–Fock and density functional systems.

Michael W. Matthew received the Ph.D. degree in applied mechanics from Yale University, New Haven, CT, in 1982, working under Dr. Peter Wegener in the area of homogeneous nucleation.

He is currently a Principal Scientist with Spectral Sciences, Inc. (SSI), Burlington, MA. He leads the technical development of the FLAASH atmospheric correction code for hyperspectral and multispectral imagery. He has also been active in the continued development of the SSI/Air Force Research Laboratory radiation transport model MODTRAN as well as the development of techniques for chemical species detection and measurement. He did postdoctoral work on ion impact effects under Dr. Lewis Friedman at Brookhaven National Laboratory before joining SSI in 1985.

David Gorodetzky received the B.A. degree (magna cum laude) in earth and planetary sciences from Washington University, St. Louis, MO, and the M.S. degree in geological sciences from the University of Colorado, Boulder, in 1990 and 1996, respectively.

He is currently a Senior Advisory Consultant in remote sensing with Research Systems, Inc. (RSI), Boulder, CO. His earliest interest in remote sensing was fostered through a summer internship at NASA Headquarters' Solar System Exploration Division while an undergraduate. He joined RSI in 1997 after working for the National Oceanic and Atmospheric Administration's National Geophysical Data Center. In his eight years at RSI, his work has focused primarily on hyperspectral data analysis, algorithm evaluation and development, atmospheric correction, sensor fusion, and ENVI software design.